Patterns of theta-synchronization over the course of a perceptual decision-making task

(Bachelorproject)

Simon J. Houtman, s1715127, s.j.houtman@student.rug.nl,
Marieke van Vugt*

April 10, 2014

Abstract

Many studies have layed out the neural correlates of perceptual decision making. It has been found that several cortical regions are involved in the decision-making process, but how the different regions interact to produce the final decision is unclear. At the beginning of the decision, the emphasis lies on shuttling information from perceptual regions to regions in which evidence accumulation takes place, while towards the end, the accumulated evidence has to be transferred to regions that implement the motor response. In EEG, interaction between brain regions is thought to be reflected in synchronization of brain oscillations. Since previous studies have shown that the dynamics of evidence accumulation for perceptual decisions is reflected in the amplitude of 4-9 Hz theta oscillations, the focus was on whether different stages of the decision process would show a shift in patterns of synchronization in this frequency band. Using two different methods of computing oscillatory synchronization, the results showed that there was indeed a difference between the set of synchronized regions at the beginning vs. the end of the decision.

1 Introduction

Perceptual decision making is the process in which a decision is made based on input stimuli resulting in a motor action. It is the process of choosing one option from a set of possible actions, given the available sensory evidence (Heekeren et al., 2008; Gold & Shadlen, 2007; Platt, 2002). Many studies have examined the neural correlates of perceptual decision-making and it is thought that several wide-spread cortical regions are involved at different stages of the decision-making process. To come to a decision, a lot of information needs to be transferred between those regions, but how those regions interact to produce the final decision is unclear. In this study, we try to reveal the interactions behind the complicated mechanisms of information transfer present in a decision by looking at synchronization.

It is thought that in the beginning of a perceptual decision, the information-processing is stimulus-oriented and that during this stage, information is transferred from visual stimulus areas to areas responsible for the accumulation and integration of sensory evidence, so called integration areas. At the end of the decision, just before the response, it is thought the brain is engaged in more response-focused processing. In this response-focused stage, information of the accumulated evidence is shuttled from integration areas to motor areas in order to prepare a response (Usher & McClelland, 2001; Siegel et al., 2011). The mapping of the sensory evidence onto the evolving action plans is thought to be mediated by large-scale oscillations in widespread networks centered in prefrontal and parietal regions and it has been proposed that the posterior parietal cortex may serve as a hub integrating the large-scale processes mediated by these networks (Siegel et al., 2011). In order to come to a decision, it is therefore necessary that a lot of information is

*University of Groningen, Department of Artificial Intelligence

transferred between these areas. Studies of brain oscillations have found that the transmission of information between local and large-scale cortical regions is reflected in synchronization of brain oscillations (Varela et al., 2001; Fries, 2009). When oscillations are synchronized, they become strong enough to be detectable on the scalp and can then be measured using scalp EEG.

Studies of perceptual-decision making have found that neuronal oscillations play an important role in cortical information processing and that oscillations in different frequency bands mediate different subprocesses of perceptual-decision making. It has for example been found that fast oscillations in the EEG signal (in the high gamma-band) within local networks reflect the encoding of sensory evidence and evolving motor plans and that synchronized oscillations at lower frequencies (low gamma- and beta-band) across large-scale cortical networks mediate the integrative processes connecting these local networks (Siegel et al., 2011). While earlier studies extensively discussed oscillations in the 28-90 Hz gamma band in the context of perceptual decision-making tasks (see Fries (2009) and Wang (2010) for detailed reviews), a growing body of evidence suggests that cortical theta oscillations might have a fundamental role in perceptual decision making. It has been found that stimuli are best perceived at certain phases of the on-going 4-9 Hz theta oscillation than at other phases (Busch & VanRullen, 2010). Also, (Womelsdorf et al., 2010) suggested that the structured retrieval of choice-relevant information around decision points might be regulated by cortical networks engaging in theta rhythmic states. A prominent finding is that the dynamics of evidence accumulation correlate most strongly with oscillations in the 4-9 Hz theta-band (van Vugt et al., 2012).

Because synchronization reflects the transmission of information and because oscillations in the theta-band reflect evidence accumulation, it seems plausible that synchronizations of theta-oscillations measured in posterior electrodes, covering occipital areas, and parietal electrodes covering integration areas should be synchronized early in the decision, while at the end, one could expect to find synchronization between electrodes covering integration areas and electrodes above motor areas. It is thus expected that the EEG data during a perceptual decision making task show a shift from stimulus-focused patterns of synchronization early in the decision, to more response-focused synchronization at the end of the decision.

In this study, we examine the patterns of theta-synchronization present at different stages of a perceptual decision. Differences between the synchronization of theta oscillations at the beginning and the end of the decision are layed out. We also examine what the effects of task difficulty are on the patterns of synchronization. The expectation is that EEG data of a perceptual decision-making task show a shift from synchronization of stimulus areas with integration areas in the beginning, to synchronization of motor areas with integration areas at the end of the decision. This work not only gives insights in the underlying synchronization as a means of information transfer between cortical regions, but also contributes to our understanding of the role of theta oscillations in human decision making.

2 Methods

In this study, two methods were used to examine the patterns of synchronization over the course of a perceptual decision-making task. The first method computes the phase-synchronization and the second method uses the coherence as a measure of synchronization. The important difference between the two methods is that the first method looks at all possible combinations of electrodes, forcing us to make a hypothesis-driven choice of a subset of electrodes to look at because of computational reasons, while the second method uses a data-driven clustering of electrodes to overcome computational issues.

2.1 Task

To examine the question of whether patterns of synchronization shift over the course of a perceptual decision-making task, EEG data of a random dot motion task (Britten et al., 1992) were analyzed. The EEG data used for this study were previously

published in van Vugt et al. (2012). In the decision-making task, participants had to judge the direction of motion (left or right) of a display of randomly moving dots of which a percentage moved to the left or right. White dots (2x2 pixels) moved on a black background in an aperture of ∼7.6 cm diameter viewed from ∼100 cm (∼4° visual angle). A subset of dots moved coherently to the left or right, whereas the rest of the dots jumped randomly from frame to frame. Motion coherence was defined as the percentage of coherently moving dots. The dot density was chosen such that individual dots could not easily be tracked (17 dots/square degree). Dots moved at a speed of approximately 7°/s. Participants had to indicate their response by pressing the "Z" key with their left index finger when dots moved to the left, or the "M" key with their right index finger when dots moved to the right.

Participants also performed a control task in which the integration of motion evidence was not necessary (non-integration condition). Trials in this condition started with dots moving entirely random (0% coherence), followed by an arrow indicating the direction of the motion.

The arrow onset time was calibrated by subtracting the average time required for pressing a button in response to a stimulus ("signal detection trials") from the RT distributions from previous blocks in the non-integration condition. This way, the dot-motion-viewing times mirrored the response time of the dots trials.

For this study only the trials with moving dots (trials of the integration condition) were selected. Arrow trials and signal detection trials were removed, because no integration was present in those trials. Trials for the easy and difficult condition were collapsed for our analyses.

2.2 Participants

Twenty-three participants (12 female; 21 right-handed; mean age 25; range 18-38) participated in the experiment in exchange for payment. The experiment was approved by the Institutional Review Board of Princeton University. Participants engaged in three separate hour-long training sessions, during which EEG was not recorded, in which they became familiar with the task. At the beginning of each training session, participants had to perform the task on a psychometric block (with fixed viewing times of 1000 ms and five different coherence levels). The performance on this psychometric block was used to determine the coherences at which the participant performed at ∼70 and 90% correct. For the remainder of the training session those coherence levels were used and the coherences from the last training session were used for two main EEG sessions, during which EEG was recorded.

2.3 EEG recordings

EEG was measured for 128 channels using Neuroscan EEG caps with a Sensorium EPA-6 amplifier. The sample rate at which the data were digitized was 1000 Hz and data were band-pass filtered from 0.02 to 300 Hz; all impedances < 30 kΩ. Cogniscan software was used for data acquisition. Channels used for the monitoring of eye movements were removed from the dataset, leaving 116 channels in total.

2.4 EEG analyses

Most of the EEG analyses were done using functions in the Fieldtrip toolbox. Fieldtrip is an open source toolbox which supplies a set of high-level functions to do MEG/EEG analysis (Oostenveld et al., 2011). All code was written in MATLAB.

2.5 Artifact detection and removal

Artifacts are effects in the EEG signal that are not produced by the brain, but emerge from activity somewhere else in the body or environment, for example activity due to line noise from electrical equipment, eye blinks or eye movements. In this study, two different kinds of artifacts were removed from the data. The data were thresholded and eye-blink artifacts were removed. Both steps are explained below in detail. Removing line noise from the data was not relevant because only the theta frequency band (4-9 Hz) was studied and line noise is present at much higher frequencies (50-60 Hz) than frequencies of the theta band.

2.5.1 Step 1: Thresholding

The first step in the rejection of artifacts was thresholding the EEG signal. By visually inspect-

ing the EEG data, the acceptable range of values for the EEG signal was chosen to be -140 mV to 140 mV. Because eye-blink artifacts always produced activation above the threshold and because those were going to be removed in a later ICA analysis, frontal electrodes were not thresholded. For all other electrodes, the trials in which the EEG data exceeded the threshold were marked as artifactual and then removed from the signals of all electrodes. Data of participants for whom more than 25% of the initial trials was rejected due to artifacts, were thought to be too weak and were removed from the dataset. Table 1 shows for each participant the percentage of removed trials due to artifacts. Data of participants 9 and 10 were removed completely.

Table 1: Percentage of trials removed due to artifacts

Participant	% trials removed
1	8.8
2	0.9
3	3.2
4	4.9
5	14.0
6	1.9
7	4.1
8	3.0
9	66.8
10	51.8
11	21.8
12	12.9
13	20.6
14	0.5
15	8.5
16	1.1
17	20.7
18	1.8
19	8.5
20	5.1
21	1.8
22	1.8
23	8.6

2.5.2 Step 2: Independent component analysis

Artifacts are usually present in the signal of multiple electrodes, because EEG electrodes include activity generated within large underlying brain areas. EEG electrodes thus often contain a lot of redundant information. It would therefore be useful to isolate artifacts based on their projection to overlapping electrode subsets. This is exactly what ICA does. ICA separates the EEG signal into components which are maximally independent of each other. This method works particularly well for eye-blink artifacts, because those artifacts have a very stereotyped temporal and spatial pattern. Eye-blinks show characteristic large deflections in frontal electrodes. The advantage of ICA is that it can isolate a wide range of artifacts to a few components while removing them from all remaining components (Makeig et al., 1996). For all participants, the eye-blinks were isolated from all other components and were then removed from the data, after which the ICA components were transformed back into the original space.

2.6 Determination of regions of interest

In this study, the main focus was on what the synchronized brain networks are during different stages of the decision-making process. It is thought that perceptual processing of a visual stimulus occurs in the beginning of the decision-making process, and that the most important components of this perceptual processing are visible in the EEG signal within 200 ms after the presentation of a stimulus (Luck, 2005; Rauss et al., 2011; Di Russo et al., 2002). We therefore chose the time interval to investigate the EEG signal related to the processing of the stimulus to be the first 200 ms after stimulus onset. The time interval for the response-related activity was chosen to be the 200 ms leading up to the response, because it is thought that at the end of the decision-making process the most important information processing is done by motor areas and because important components of the preparation of a motor response, like the pre-motion positivity (positive activity peak at 100 ms before the response) and motor potential (activity peak at 40-10 ms before the response),

are usually visible in the response-related activity within 200 ms prior to the response (Deecke et al., 1969).

Because of the assumption that early in the decision the information processing is focused on the processing of the visual stimulus, it is expected that posterior electrodes covering regions of the visual cortex should show activity peaks in the beginning of the decision, and because it is thought that at the end of the decision the information processing is response-focused, it is expected that central electrodes covering motor areas should show activity peaks at the end of the decision.
To check the assumptions that early in the decision posterior electrodes covering the visual cortex and at the end of the decision central electrodes covering motor areas should show activity peaks, the event-related potentials (ERP) were computed for the stimulus-related EEG activity and the response-related EEG activity. An ERP is the average of EEG activity time-locked to a sensory, cognitive or motor event (Coles & Rugg, 1995). To compute the stimulus-locked ERP, all trials for a participant were aligned at stimulus onset and the stimulus-locked ERP for a participant was then computed by averaging over all trials for the time interval of 200 ms after stimulus onset. To compute the response-locked ERP, the trials were aligned at the response, because the reaction time of a participant differed for every trial. The response-locked ERP was then computed by averaging over all response-aligned trials, using the time interval of 200 ms before the response. To determine the general brain state at the time of stimulus onset and response production, the grand average ERP was computed for the stimulus-locked event and the response-locked event, which is the average ERP signal over all electrodes, all trials and all participants. Also, topoplots of the stimulus-locked and response-locked ERPs were made to investigate which electrodes show activity during those time-locked events.

2.7 Computation of phase-synchronization

The first method that was used to investigate the patterns of synchronization computes the phase synchronization between the EEG signals. Phase synchronization measures the relation of the temporal structures of the signals regardless of signal amplitude. Two signals are phase-synchronized when they enter into phase-locking over a period of time (Lachaux et al., 1999). To compute the phase-locking between the EEG signals and to determine which phase-locking values were significant, we implemented phase-locking statistics (PLS) described in Lachaux et al. (1999, 2000). In the first step of PLS, the instantaneous phase is computed for signals x and y of every electrode combination (x, y). Next, phase-locking values are computed by averaging the phase difference between the signals over all trials. Third, phase-locking statistics are determined by comparing the original phase-locking values to a set of surrogate phase-locking values (pseudo-random phase-locking values).

2.7.1 Computation of instantaneous phase

In order to compute the phase-locking of signals, the phase and amplitude had to be separated. One way to extract the phase from a signal is by convolving the EEG signal with a Gabor or Morlet wavelet. The data was wavelet-transformed in the theta (4-9 Hz) frequency band using six-cycle Morlet wavelets. Morlet wavelets were used because they are well-suited for analyzing human EEG data, because the sinusoidal shape of the wavelet, which tapers at the end, matches the signal one expects to extract from the EEG signal (Schiff et al., 1994). Furthermore, Morlet wavelets have an optimal trade-off between temporal and frequency resolution for EEG data (van Vugt et al., 2007). Six-cycles are often used for the analysis of EEG data (Caplan et al., 2001).
Morlet wavelets were computed using the Fieldtrip function $ft\_freqanalysis$. After the transformation of the EEG signals with the Morlet wavelet, the phase of the signals was extracted from the coefficients of their wavelet transform.

2.7.2 Computation of phase-locking values

The phase-locking value (PLV) between two signals x and y measures the variability of the phase difference at time t and frequency f over all trials:

$$PLV(f,t) = |\frac{1}{N_{trial}} \sum_{trial=1}^{N_{trial}} \exp(j(\phi_y, trial(f,\tau) - \phi_x, trial(f,\tau)))| \quad (2.1)$$

where ϕ is the phase and N_{trial} is the total number of trials. By dividing the sum of the phase differences of all trials over the total number of trials, the PLV has a normalized index. If the difference in phase between the signals is approximately the same for all trials, the average difference will be close to zero, and PLV will be close to 1 ($PLV = 1$ when phases are perfectly phase-locked). If the phase difference varies a lot across the trials, PLV will be close to zero. The code to compute the phase-locking values can be found in Appendix A.

2.7.3 Computation of surrogate phase-locking values

Surrogate phase-locking values were computed from the same signals x and y, but after permuting the order of the trials in y. This way, surrogate data were created with the same distribution and characteristics as the original signals but without any connection between the signals x and y. Twenty-four electrodes were used in the computation of surrogate phase-locking values instead of all 116 electrodes because of memory limitations (Computing 200 surrogate phase-locking values for 13456 electrode combinations was not possible). The selected electrodes were: 91, 92, AF7, AF8, F3, F4, FZ, FC3, FC4, C5, CZ, C6, 120, 69, P5, PZ, P6, 110, 112, O1, O2, 101, 106, 124, covering the major areas of the scalp. For every electrode combination (x, y), the phase-locking value between x and y was computed, and 200 different permutations of y were created to compute a set of 200 surrogate phase-locking values.

Phase-locking statistics were then computed by comparing the original PLV to the 200 surrogate phase-locking values of the corresponding electrode combination. A significant PLV should be larger than most of the distribution of surrogate PLVs. Because the computation of the significance of the PLV between all combinations of 24 electrodes involved many t-tests, a False Discovery Rate procedure was used to compute the significance level of $p = 0.005$. A False Discovery Rate procedure is a statistical method to correct for multiple comparisons. The False Discovery Rate is a method to correct for multiple comparisons, but this method is much less stringent on a false discovery than common multiple comparisons methods like the Bonferonni correction, but which at the same time has much larger power than a Bonferonni correction, especially for a great amount of comparisons (Benjamini & Hochberg, 1995). A False Discovery Rate of 0.01 was used, which indicates that on average 1 in 100 of the significant effects that are found is a false positive. The code to compute surrogate phase-locking values and phase-locking statistics can be found in Appendix B.

2.8 EEG coherence analysis: FuMapLab

A second method was used to explore the patterns of synchronization over the course of a perceptual decision-making task. For this second method, instead of using the phase-locking value as a measure of synchrony, the coherence measure was used. A data-driven approach was chosen to overcome the computational constraints encountered in the hypothesis-driven method for the computation of the phase-synchronization. We used the method from ten Caat et al. (2007), who developed a data-driven method for the computation and visualization of high-density EEG coherence using functional units (FUs) as regions of interest. The method is implemented in FuMapLab, which is a Matlab toolbox for the visual analysis of multichannel EEG coherence (ten Caat et al., 2008).

2.8.1 Computation of functional units for individual participants

Because the oscillations of a single source are usually recorded by multiple EEG electrodes, it makes sense to first compute sets of multiple electrodes which are spatially connected and which record similar signals, called functional units, and then compute the connections between those functional units. This is exactly what FuMapLab does. Without the intention of describing the graph theory behind FuMapLab in full, a few basic steps in the procedure are pointed out.

FuMapLab starts with computing the coherence graph for every participant. This is a graph in which electrodes are represented by vertices and significant coherences between electrodes are represented by edges. Significant coherences were determined by comparing the coherence values to a significance threshold. The significance threshold for the coherence is given by $\theta = 1 - p^{1/(L-1)}$ in which L is the amount of trials for the participant and p is a probability value associated with a confidence level α, such that $p = 1 - \alpha$ (ten Caat et al., 2007). For this study, the dataset for each participant consisted of 50 trials ($L = 50$). Trials were selected based on the corresponding response time. We only selected trials for which the response time was below 1000 ms, because a high response time for a trial might indicate that the participant was distracted from the task at hand. The same probability value was used as in the computation of significant phase-locking values: $p = 0.005$, which resulted in a coherence threshold of $\theta = 1 - 0.005^{1/(50-1)} = 0.1025$.

After the computation of significant coherences between all electrodes, the functional units were computed. A FU is represented in the EEG coherence graph by a set of spatially connected vertices which form a 'clique'. A clique is a subset of electrodes in which all electrodes are connected to each other, based on whether or not the coherence between the two electrodes crosses a significance threshold. In order to compute the functional units, the spatial relationships between the electrodes had to be determined first. This is done in FuMapLab by partitioning the space of electrodes into a number of cells using a Voronoi diagram. Each cell is a region with one electrode as a center and the cell encloses all points which are closest to this center electrode. Two cells are neighbors if they have a boundary in common. After the computation of the spatial relationships between all electrodes, functional units were detected based on a maximal clique-based method, which means that FUs were detected which are as large as possible. Every cell was allowed to be part of one functional unit. For a complete description of how the functional units were computed using the maximal clique-based method, the reader is referred to the paper of ten Caat et al. (2007). To find the overall patterns of coherence in the coherence graph of an individual participant, connections between all functional units were computed. To compute which inter-FU connections were significant, the same coherence threshold was used as for the determination of the initial coherences.

2.8.2 Visualizing the functional units

After the computation of the connections between the functional units, FuMapLab visualizes the FUs in a so called FU map. In such a map, each FU is visualized as a set of cells with the same gray value, and different gray values for different functional units. If the coherence between two functional units exceeded significance threshold, a line was drawn between the centers of the functional units. The significance threshold was consistently chosen to be equal to the significance threshold of the individual coherences.

2.8.3 Group analysis

After the analysis of EEG coherence for individual participants, FuMapLab performs a group analysis to investigate the general patterns of EEG coherence over all participants. First, the group mean coherence was computed by taking the mean of the coherences for all electrode pairs over all participants. The group mean coherence was then visualized by plotting a group mean coherence map. Only the edges with a coherence value greater than the coherence threshold were plotted. Once again, the same threshold was used as for the individual coherences (ten Caat et al., 2008). Second, the group FU size map was computed which visualizes the average FU size for every electrode across a collection of individual FU maps, which emphasizes those electrodes that are often part of a large FU in the individual subjects (ten Caat et al., 2008).

3 Results

3.1 Event-related potentials for the stimulus-processing interval and response interval

First the assumption was tested that early in the decision, information processing should take place in visual stimulus areas and that at the end of the decision, just before the response, the information

processing should be found in motor areas. If this assumption is correct, we should find the focus of activity in posterior electrodes at the beginning of the decision, covering visual stimulus areas and at the end, we should find activity in central and parietal electrodes, covering motor areas.
Figure 1 shows the stimulus-locked and response-locked event-related potentials, with corresponding topoplots. In Figure 1A, the grand average stimulus-locked ERP (in μV) is plotted for the first 200 ms after stimulus onset. Two activity peaks are present in the stimulus-locked ERP: One negative activity peak around ∼120-130 ms, and one positive peak of activation at ∼150-170 ms. These activation peaks are possibly related to motion onset. These results correspond to evidence from previous studies, which found that two activity peaks related to motion onset should be visible in a motion discrimination task in the first 200 ms after stimulus onset (Kuba & Kubová, 1992; Prieto et al., 2007). Figure 1B shows the topoplot corresponding to the stimulus-locked ERP. The focus of activation peaks is mainly found in posterior electrodes, covering occipital areas. The grand average response-locked ERP is shown in Figure 1C. The course of the response-locked ERP shows a drop of activity around ∼100 ms before the response. After this negative peak, theta power increases until just before the response, after which the power decreases, consistent with results of earlier studies (Jacobs et al., 2006; Deecke et al., 1969). Figure 1D shows the topoplot for the response-locked ERP. The focus of activity for the response-locked ERP is found above central and parietal electrodes, as expected. These results confirm the assumption that posterior electrodes should show activity peaks at the beginning and that central and parietal electrodes should show activity peaks at the end of the decision, reflecting stimulus-related processing at the beginning and response-focused processing at the end of the decision.

3.2 Relationship between PLV and PLS

Before launching into the analysis of phase synchronization in the beginning and end of the decision, the relationship between the phase-locking values and the phase-locking statistics was analyzed to check if the results matches the expected outcome. If the method presented in this study is correct, an increasing PLV should be accompanied by an increasing significance of the PLV, and therefore lower values of PLS.
The bottom plot in Figure 2 shows the relationship between the values of PLV and the values of PLS. As one can see, PLS decreases as PLV increases, as expected. The top left figure in Figure 2 shows the phase waveforms of two signals x and y for which a low PLV was found ($PLV = 0.1761$). The waveforms oscillate out of phase, consistent with the assumption that two waveforms that oscillate out of phase should have a low phase-locking. The top right figure in Figure 2 shows two signals for which a high PLV was found ($PLV = 0.8223$). The waveforms show a high phase-locking, which is to be expected when a high PLV is found. These results confirm that phase-locking statistics is a viable method to compute phase synchronization.

3.3 Phase synchronization for the beginning and end of the decision

After having confirmed that the method to compute phase synchronization works, the patterns of phase synchronization were analyzed by examining topoplots of significantly phase-locked electrode combinations. We will first describe the results by visually inspecting the topoplots for the different conditions of task difficulty for the beginning and end of the decision, after which the differences will be tested formally. The expectation was that we should find strong phase-locked connections between electrodes above stimulus areas and integration areas early in the decision, and that we should find strong connections between integration areas and motor areas towards the end of the decision.
Figure 3 shows the topoplots for the beginning of the decision (0 - 200 ms after stimulus onset, left column) and end of the decision (200 ms previous to the response, right column) for electrode combinations for which a significant phase-locking statistic was found. The color of a connection between two electrodes indicates the strength of the phase-locking value. Only phase-locking values larger than 0.4 were plotted. The first row shows the topoplots for the high

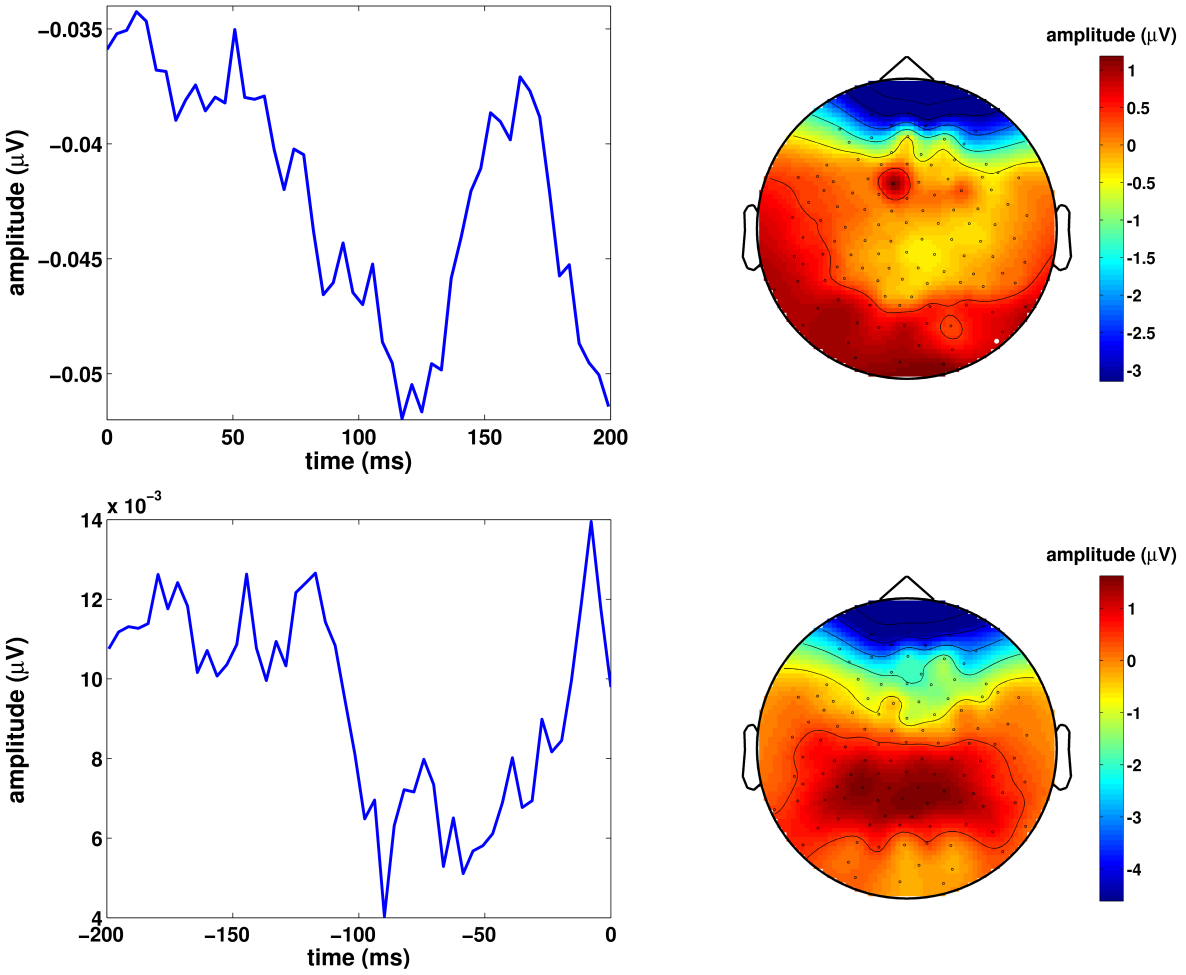

Figure 1: Stimulus and response-locked event-related potentials (ERPs) (A) Grand average stimulus-locked ERP (i.e. average across all electrodes, all trials and all participants, 0 - 200 ms after stimulus onset). (B) Topographic plot of ERP amplitude for the stimulus-locked ERP in (A). (C) Grand average response-locked ERP (time interval of 200 ms previous to the response). (D) Topographic plot of ERP amplitude for the response-locked ERP in (C).

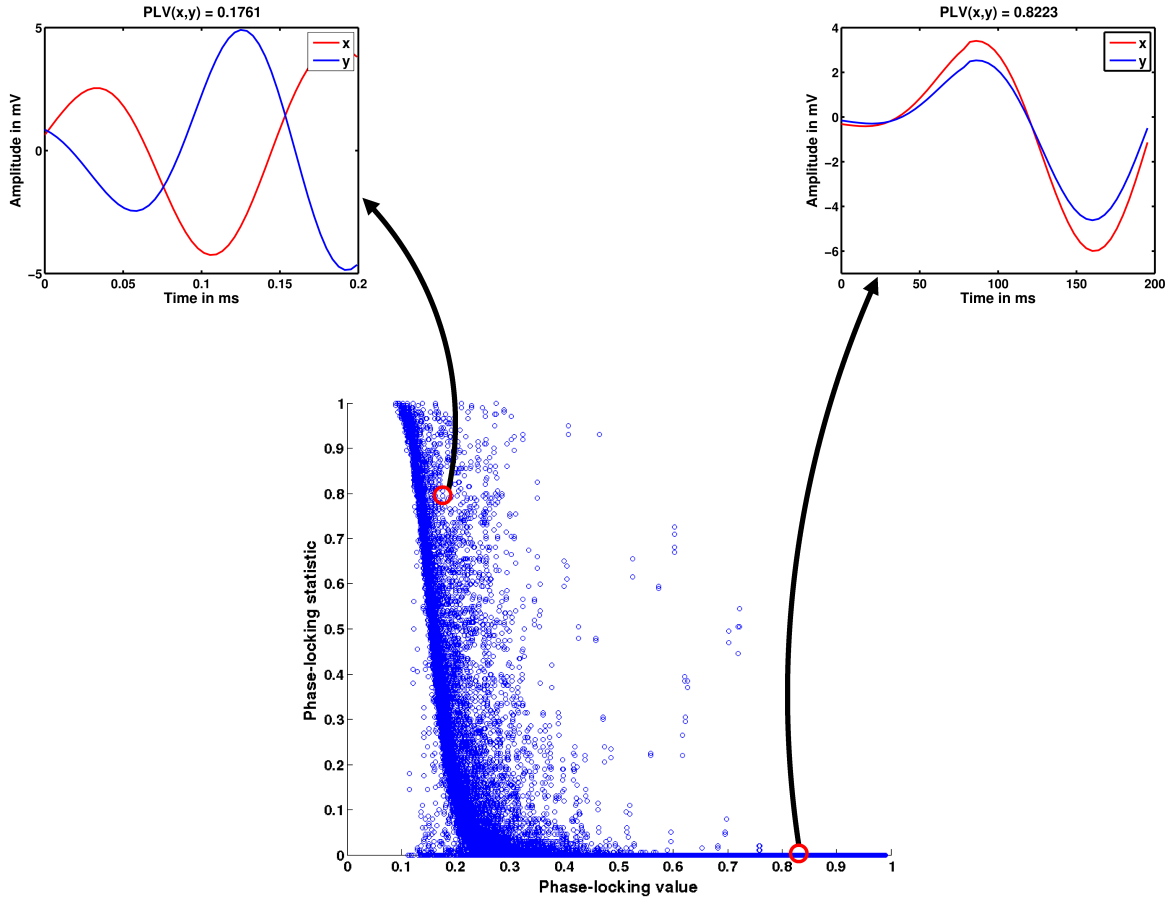

Figure 2: Relationship between the PLV and PLS (bottom plot) with the least-squares line through all values of PLS (red). Two signals x and y are shown for a low phase-locking between the signals (top left, $PLV = 0.1761$) and for a high phase-locking between the signals (top right, $PLV = 0.8223$).

coherence (easy) condition. The topoplots for the low coherence (hard) condition are shown in the second row. At first sight, the topoplots seem to resemble each other a lot. However, there are important differences when we look at the details. We first notice that in the high coherence (easy) condition, more combinations of electrodes show significant phase-locking than in the low coherence (hard) condition. This is rather unexpected. One would expect more synchronization in general for the low coherence condition, because the task is harder than for the high coherence condition, and so more evidence accumulation needs to take place.

For both the beginning and end of the decision, a few connections with strong phase-locking ($PLV > 0.7$) were found between electrodes above occipital, parietal and frontal areas. However, the more interesting connections of phase-synchronization were found for phase-locking values between 0.4 and 0.7. For example, as we can see from the topoplots for the low coherence condition, more electrode pairs above parietal areas show significant phase-locking than at the end. Furthermore, the connections between parietal electrodes which are significantly phase-locked both in the beginning and at the end have a higher phase-locking at the beginning, indicated by colors higher on the colorbar. These strong parietal connections possibly reflect the processing of the stimulus and the accumulation of evidence in integration areas in the beginning of the decision. For the high coher-

ence condition, more significant connections were found above parietal areas at the end with respect to the beginning of the decision, but all connections were weaker at the end than at the beginning. At the end of the decision, more significant connections are found between parietal electrodes and medial-frontal electrodes, possibly above motor areas, with respect to the beginning. Connections between electrodes above occipital areas and parietal areas are approximately the same for both the beginning and end of the decision, although the connections were stronger in the beginning of the decision. These results show that electrodes above integration areas show stronger synchronization in the beginning than at the end of the decision, and that connections between electrodes above integration areas and motor areas show stronger synchronization at the end of the decision. Thus, the results are in agreement with our hypothesis that states there is a shift from stimulus-focused processing in the beginning, to more response-focused processing at the end of the decision, visible in the phase synchronization of oscillations in the theta frequency band.

3.3.1 Differences of phase synchronization between the beginning and end of the decision

After the patterns of theta-synchronization were computed, we wanted to compare the differences between the early and the late interval and between the two task difficulties more directly. For every electrode combination, we performed a 2x2 repeated measures analysis of variance (ANOVA) on the mean phase-locking value over all participants. The factors were stage (begin / early) and motion coherence (low / high). For 448 (out of 13456) electrode combinations a significant effect of stage was found (i.e. a significant difference between the beginning and the end of the decision). Again, because of the many comparisons, we computed the significance level using a False Discovery Rate (0.001, i.e. 1 in 1000 found differences is a false positive) which resulted in a p-value threshold of $p = 1.6173 * 10^{-5}$. No significant effects of motion coherence were found on the phase-locking value. Also, there were no interaction effects of stage and motion coherence.
Figure 4 shows the topoplot for all electrode combinations for which a significant difference was found for the phase-locking value between the beginning and end of the decision. The differences were plotted in such a way that for every electrode combination it could be identified whether the phase-locking was higher at the beginning or at the end of the decision. This was done by plotting significant differences in two colors: A red line whenever the phase-locking value for the electrode combination was higher in the beginning compared to the end of the decision. A blue line means that the phase-locking value was higher at the end with respect to the beginning of the decision. The expectation was that we should find a shift from synchronization between stimulus-areas and integration areas in the beginning to synchronization between motor areas and integration areas at the end of the decision. This should be visible in the topoplot of the difference of the phase-locking value by red lines between posterior and parietal electrodes, and blue lines between central and parietal electrodes.
The majority of red lines are found between electrodes covering occipital areas and prefrontal electrodes, indicating that these connections are more phase-synchronized in the beginning with respect to the end of the decision. Blue lines are mainly found between electrodes covering motor areas with other electrodes above motor or parietal areas, as well as with electrodes above prefrontal areas and parietal areas, indicating that these connections are more phase-synchronized at the of the decision with respect to the beginning. These results suggest that information is transferred from visual stimulus areas to prefrontal areas in the beginning of the decision, and that information is transferred between motor areas and between motor and parietal areas at the end of the decision.

3.4 EEG coherence analysis

Finally, the coherence measures over the course of the decision were analyzed. The FU maps are shown for functional units containing at least 6 cells. Figure 5 shows the group FU maps with significant connections between the functional units for the group mean coherence. The color of the connection indicates the strength of the inter-FU coherence. Different functional units have different gray values. The left column in Figure 5 shows the FU maps for the beginning of the decision and the

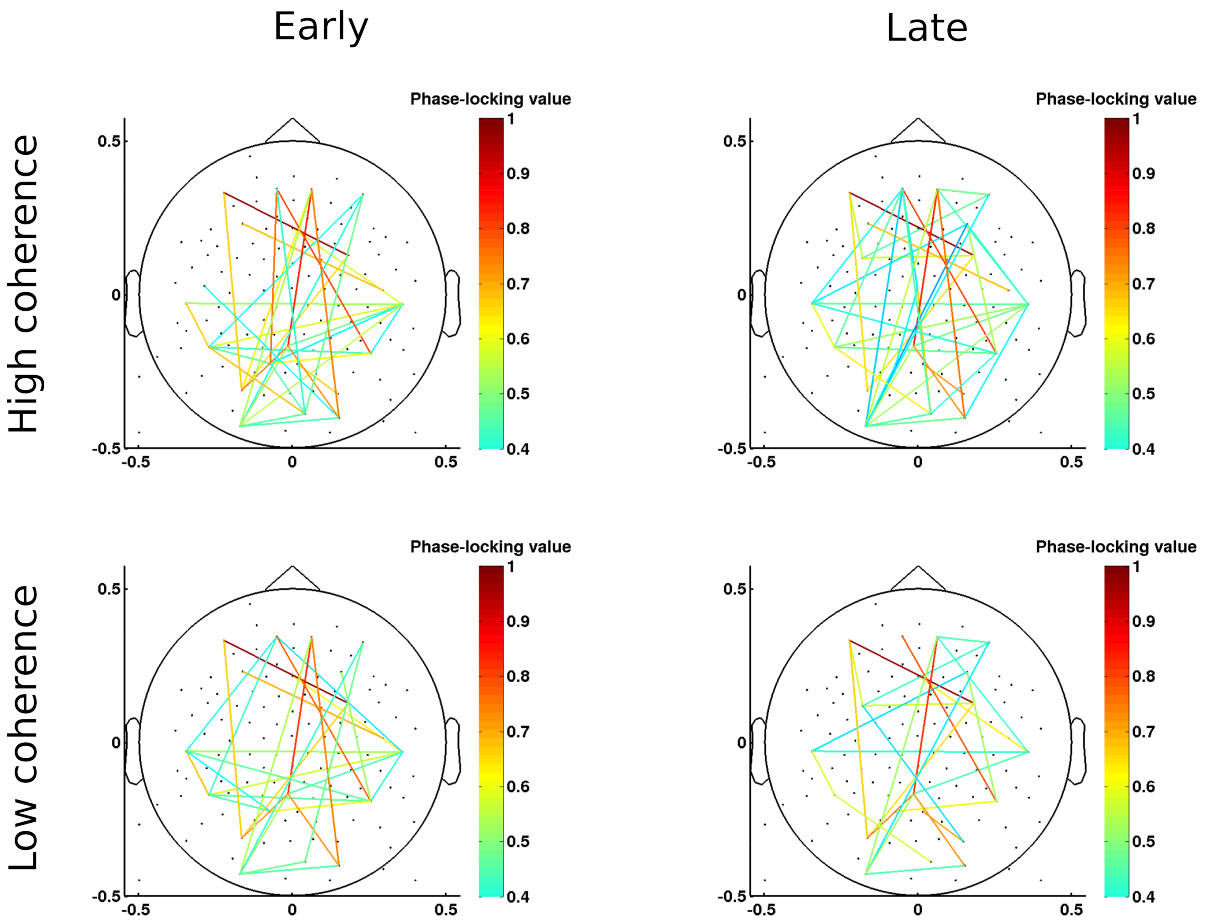

Figure 3: Topoplots showing the connections between significantly phase-locked electrodes for the stimulus-processing interval (left column) and response interval (right column). The first row shows the topoplots for the high coherence (easy) condition. The second row shows the topoplots for the low coherence (hard) condition. The color of a connection between two electrodes indicates the strength of the phase-locking value. Phase-locking statistics were computed by determining the fraction of surrogate phase-locking values that were bigger than the original phase-locking value. The significance of the PLV was determined by comparing the phase-locking statistics to a significance threshold of 0.005, which was computed using a False Discovery Rate (fdr = 0.01). 24 electrodes were used in the computation. Electrode combinations with a PLV $>$ 0.4 were plotted.

right column shows the FU maps for the end of the decision. Three large and four smaller functional units are visible in the FU maps of both conditions for the beginning of the decision and in the FU map for the low coherence condition for the end of the decision. The FU map for the high coherence condition for the end of the decision shows four large functional units and five smaller functional units.

Early in the decision, significant connections are found between a large posterior FU and a large frontal functional unit, between the large posterior FU and small lateralized FUs to the left and to the right of the head and between the lateralized FUs themselves. The large posterior FU possibly reflects the coherence of visual stimulus areas. The two small functional units at both sides of the head are possibly above integration areas, responsible for evidence accumulation. The medium-sized functional unit in the center is possibly related to the preparation of a motor action. For the low coherence con-

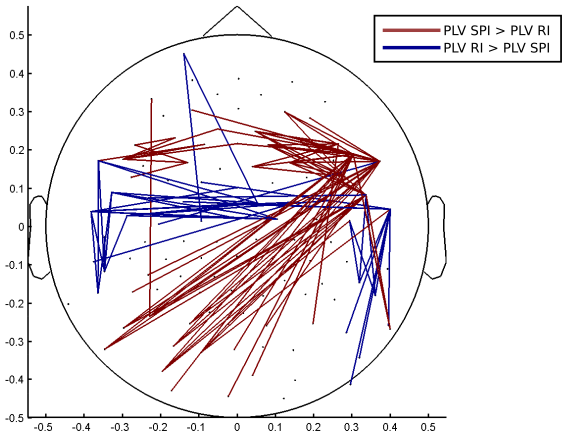

Figure 4: Topoplot showing the electrode combinations for which a significant difference for the phase-locking value (PLV) was found between the stimulus-processing interval and the response interval. The significance level was computed using a False Discovery Rate procedure (fdr = 0.001). Red lines indicate that the PLV was higher in the stimulus-processing interval with respect to the response interval. Blue lines indicate that the PLV was higher in the response interval when compared to the stimulus-processing interval.

dition, we found the same patterns of coherence for the end of the decision as at the beginning of the decision. For the high coherence condition, a lot more significant connections (21) were found at the end than at the beginning (10). This could be because a large part of the brain is activated around the time of a response in a decision-making task, as suggested by earlier research (Jacobs et al., 2006). However, this phenomenon was not found in the low coherence condition. The last important note is that more connections are present in the low coherence condition than in the high coherence condition, which could be because the difficulty of the task was higher, but this was only visible for the beginning of the decision and not at the end.

4 Conclusion and discussion

In this study, the patterns of theta-synchronization over the course of a perceptual-decision making task were investigated. The most important finding is that EEG oscillations in the theta-band show a shift of patterns of synchronization from stimulus-focused processing in the beginning, to more response-focused processing at the end of a perceptual decision-making task.
From the analysis of the stimulus-locked ERP and response-locked ERP it can be concluded that early in the decision, cortical information processing mainly takes place in visual stimulus areas and that at the end of the decision, cortical information processing is more focused to motor areas for oscillations in the theta frequency band.
In this study, we implemented a powerful method (PLS) to compute significant phase-synchronization between EEG electrodes. Although the overall pattern of phase-synchronization was approximately the same for the beginning and the end of the decision, important differences were found between the two stages of the decision. The differences between the beginning and end showed us that synchronization of electrodes above visual stimulus areas and frontal regions was larger in the beginning than at the end of the decision. The synchronizations in the beginning were not between visual stimulus areas and parietal areas as expected, but between visual stimulus areas and frontal regions. It could be that the connections of phase synchronization we found in the beginning of the decision are between visual stimulus areas and the dorsolateral prefrontal cortex or frontal eye field, which have previously been indicated as important areas responsible for controlling the flexible mapping of sensory evidence onto motor plans (Siegel et al., 2011). The phase-synchronized connections above motor areas and between motor areas and integration areas were stronger at the end with respect to the beginning of the decision. However, these difference were not reflected by the patterns of the EEG coherence measure.
We therefore conclude that a shift of phase-synchronization of theta oscillations does take place from synchronization between visual stimulus areas and frontal regions in the beginning, to synchronization between motor areas and integration areas at the end of the decision.

An important point to discuss is the hypothesis-driven choice of the electrodes for which we computed the phase-locking statistics. Because we could not compute the phase-locking statistics

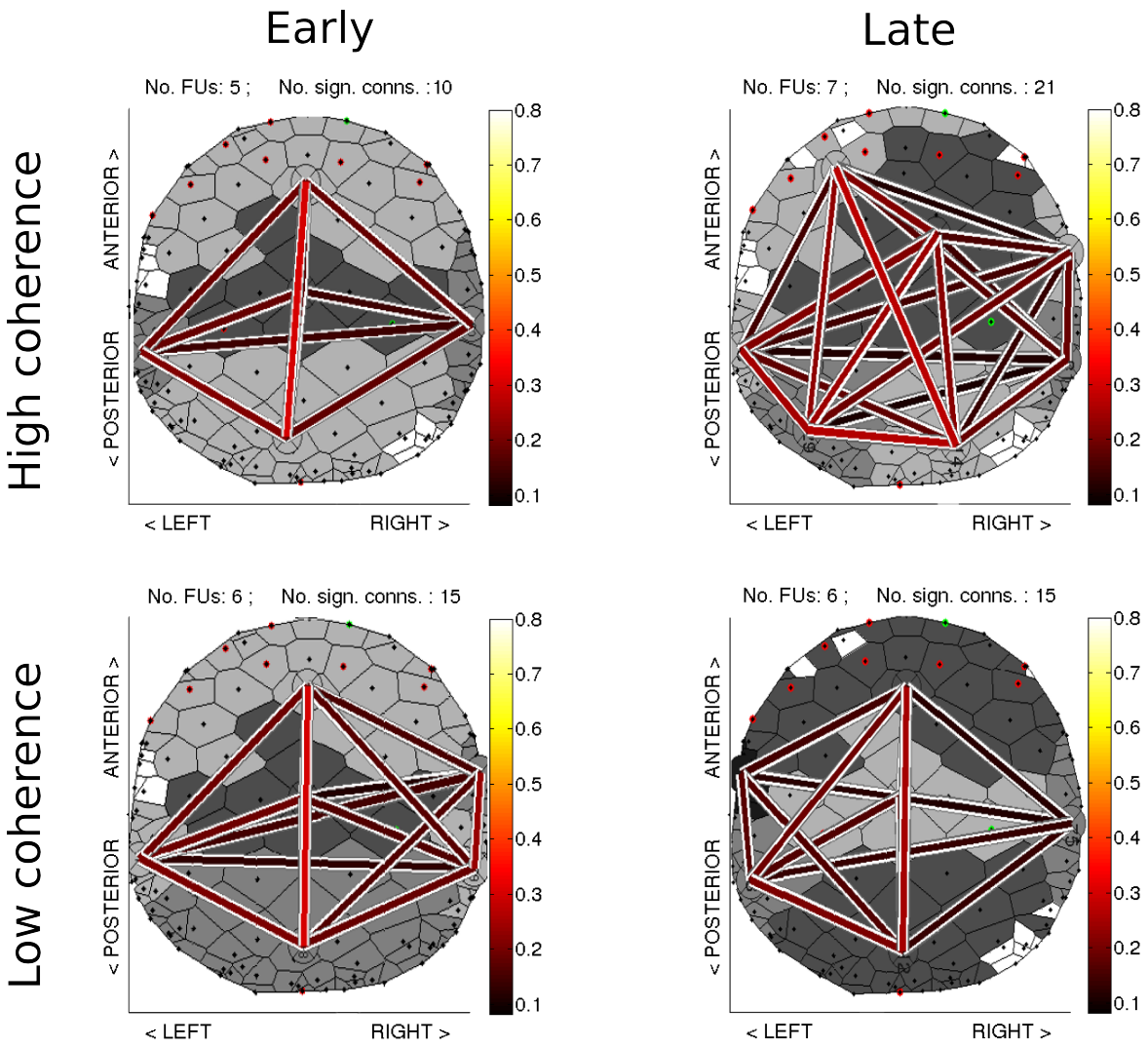

Figure 5: Group Functional Unit maps (EEG theta frequency band 4-9 Hz) of 21 participants. The first row shows the FU maps for the high coherence (easy) condition. The second row shows the FU maps for the low coherence (hard) condition. The left column shows the FU maps for the beginning of the decision (0 - 200 ms after stimulus onset). The right column shows the FU maps for the end of the decision. Different Functional Units have different gray values. The data of each participant consisted of 50 trials. The coherence threshold to compute the functional units ($\theta = 0.1025$) was determined using a p-value of 0.005 (the same as for the computation of significant phase-locking values). The minimum size of a functional unit was 6 cells. Lines show connections between FU centers, if the inter-FU coherence exceeds the significance threshold. The color of the line indicates the strength of the inter-FU coherence (see color bar at the right of the FU map). The number of functional units and the number of significant inter-FU connections are displayed above each FU map. At the center of each FU a circle is drawn with a number inside, which shows the strength of the FU.

for all combinations of 116 electrodes because of memory issues, we had to make a choice of electrodes to investigate. One could argue that the expected patterns of synchronization present during the decision are not reflected well by the phase-locking between the specific electrodes we chose to look at. However, it is unlikely that the overall patterns would change a lot if we would choose another set of electrodes (also covering the whole scalp), because the data-driven method which we used to compute the coherence also did not yield the expected overall patterns. Future studies could develop a data-driven method to compute phase-synchronization like the data-driven coherence method which does not suffer of memory issues.

Another point for discussion is the length of the time intervals. The time intervals had a length of 200 ms. We only looked at low frequencies (4-9) Hz. The lowest frequency of 4 Hz only has 4/5 of a cycle within 200 ms, and the highest frequency of 9 Hz has less than 2 cycles within 200 ms. The phase-locking value was defined as the measure of stability of the phase-locking between signals over a specific time interval. It could be that the stability of the phase-locking value changes if we would, for example, look at a time interval of 400 ms instead of 200 ms. Future studies should investigate the behavior of the phase-locking value in relation to different lengths of time intervals. Also, the phase synchronization could be studied for theta oscillations for larger time windows.

It is also important to consider alternative explanations for the differences we found for the phase-synchronization between the beginning and the end of the decision. For example, another interpretation could be that the phase-synchronization reflects uncertainty of the participant instead of information transfer. One could also argue that the patterns of phase-synchronization we found in this study are related to the timing of pressing the button.

As a last note, it is important to state that our results merely show a correlation between phase synchronization and information transfer. It could be possible that the differences in synchronization are merely epiphenomenal. In order to come to more causal claims about the role of synchronization in information transfer, we would need to add a control condition in which we turn off synchronization. Further research could identify the causal relationships between phase synchronization and information transfer during decision making.

In this study, we found a difference between the set of synchronized regions in the beginning and the set of synchronized regions at the end of the decision. We showed that there is a shift from synchronization of visual stimulus areas with integration areas in the beginning of the decision, to synchronization of motor areas with integration areas at the end of the decision, for oscillations of the theta frequency band. This study is one of the first studies to start to elucidate the patterns of synchronization in decision making. Our results add to the knowledge of the complex large-scale interactions between brain areas during perceptual decision making and also gives insights in the role of theta oscillations in human decision making.

References

Benjamini, Y., & Hochberg, Y. (1995). Controlling the false discovery rate: A practical and powerful approach to multiple testing. *Journal of the Royal Statistical Society. Series B (Methodological)*, *57*(1), pp. 289-300.

Busch, N. A., & VanRullen, R. (2010). Spontaneous EEG oscillations reveal periodic sampling of visual attention. *Proceedings of the National Academy of Sciences*, *107*, 16048-16053.

Caplan, J. B., Madsen, J. R., Raghavachari, S., & Kahana, M. J. (2001). Distinct patterns of brain oscillations underlie two basic parameters of human maze learning. *Journal of Neurophysiology*, *Jul*(86), 368-380.

Coles, M. G. H., & Rugg, M. D. (1995). Event-related brain potentials: An introduction. *Electrophysiology of Mind: Event-Related Brain Potentials and Cognition*, 1-26.

Deecke, L., Scheid, P., & Kornhuber, H. H. (1969). Distribution of readiness potential, pre-motion positivity, and motor potential of the human cerebral cortex preceding voluntary finger movements. *Experimental Brain Research*, *7*(2), 158–168.

Di Russo, F., Martínez, A., Sereno, M. I., Pitzalis, S., & Hillyard, S. A. (2002). Cortical sources of the early components of the visual evoked potential. *Human brain mapping*, *15*(2), 95–111.

Fries, P. (2009). Neuronal gamma-band synchronization as a fundamental process in cortical computation. *Annual Review of Neuroscience*, *32*, 209-224.

Gold, J. I., & Shadlen, M. N. (2007). The neural basis of decision making. *Annual Review of Neuroscience*, *30*(1), 535–574.

Heekeren, H. R., Marrett, S., & Ungerleider, L. G. (2008). The neural systems that mediate human perceptual decision making. *Nature Reviews Neuroscience*, *9*(6), 467-479.

Jacobs, J., Hwang, G., Curran, T., & Kahana, M. J. (2006). EEG oscillations and recognition memory: theta correlates of memory retrieval and decision making. *Neuroimage*, *32*(2), 978–987.

Kuba, M., & Kubová, Z. (1992). Visual evoked-potentials specific for motion-onset. *Documenta Ophthalmologica*, *80*, 83-89.

Lachaux, J., Rodriguez, E., Martinerie, J., & Varela, F. (1999). Measuring phase synchrony in brain signals. *Human brain mapping*, *8*(4), 194-208.

Lachaux, J., Rodriguez, E., van Quyen Le, Lutz, A., Martinerie, J., & Varela, F. J. (2000). Studying single-trials of phase synchronous activity in the brain. *International Journal of Bifurcation and Chaos*, *10*(10), 2429-2439.

Luck, S. J. (2005). *An introduction to the event-related potential technique.* MIT press Cambridge, MA:.

Makeig, S., Bell, A. J., Jung, T.-P., & Sejnowski, T. J. (1996). Independent component analysis of electroencephalographic data. *in Advances in Neural Information Processing Systems*, 145-151.

Oostenveld, R., Fries, P., Maris, E., & Schoffelen, J. (2011). Fieldtrip: Open source software for advanced analysis of MEG, EEG, and invasive electrophysiological data. *Computational Intelligence and Neuroscience*, *2011*.

Platt, M. L. (2002). Neural correlates of decisions. *Current Opinion in Neurobiology*, *12*(2), 141-148.

Prieto, E. A., Barnikol, U. B., Soler, E. P., Dolan, K., Hesselmann, G., Mohlberg, H., ... Tass, P. A. (2007). Timing of V1/V2 and V5+ activations during coherent motion of dots: An MEG study. , *37*(4), 1384-1395.

Rauss, K., Schwartz, S., & Pourtois, G. (2011). Top-down effects on early visual processing in humans: a predictive coding framework. *Neuroscience & Biobehavioral Reviews*, *35*(5), 1237–1253.

Schiff, S. J., Aldroubi, A., Unser, M., & Sato, S. (1994). Fast wavelet transformation of EEG. *Electroencephalography and Clinical Neurophysiology*, *91*(6), 442-455.

Siegel, M., Engel, A. K., & Donner, T. H. (2011). Cortical network dynamics of perceptual decision-making in the human brain. *Frontiers in Human Neuroscience*, *5*, 21.

ten Caat, M., Maurits, N. M., & Roerdink, J. B. T. M. (2007). Functional unit maps for data-driven visualization of high-density EEG coherence. In *Eurographics/IEEE VGTC symposium on visualization (eurovis)* (p. 259-266).

ten Caat, M., Maurits, N. M., & Roerdink, J. B. T. M. (2008). Data-driven visualization and group analysis of multichannel EEG coherence with functional units. *IEEE Trans. Visualization and Computer Graphics*, *14*(4), 756–771.

Usher, M., & McClelland, J. L. (2001). The time course of perceptual choice: The leaky, competing accumulator model. *Psychological review*, *108*(3), 550-592.

van Vugt, M. K., Sederberg, P. B., & Kahana, M. J. (2007). Comparison of spectral analysis methods for characterizing brain oscillations. *Journal of Neuroscience Methods*, *162*, 49-63.

van Vugt, M. K., Simen, P., Nystrom, L. E., Holmes, P., & Cohen, J. D. (2012). EEG oscillations reveal neural correlates of evidence accumulation. *Frontiers in Human Neuroscience*, *6*(106).

Varela, F., Lachaux, J.-P., Rodriguez, E., & Martinerie, J. (2001). The brainweb: Phase synchronization and large-scale integration. *Nature Reviews Neuroscience*, *2*(4), 229–239.

Wang, X.-J. J. (2010). Neurophysiological and computational principles of cortical rhythms in cognition. *Physiological reviews*, *90*(3), 1195–1268.

Womelsdorf, T., Vinck, M., Leung, L. S., & Everling, S. (2010). Selective theta-synchronization of choice-relevant information subserves goal-directed behavior. *Frontiers in human neuroscience*, *4*.

Appendix A: computePLV.m

Function to compute phase-locking values. The input signal is a wavelet of an EEG signal in Fieldtrip format. The output is a data structure with the phase-locking values stored in *PLV.plvspctrm*, a 4D-matrix with the following dimension order: <channel x channel x frequency x time>.

```
function PLV = computePLV(wavelet)
    % Computes phase-locking values for all <channel x channel> combinations
    % for a wavelet of an EEG signal in Fieldtrip format
    %
    % Input parameters:
    % wavelet = Morlet wavelet of EEG signal in Fieldtrip format
    % Dimord of input wavelet: <trials x channel x frequency x time>
    %
    % Output parameters:
    % PLV = A data structure with the phase-locking values stored in the
    % field: PLV.plvspctrm, a 4D-matrix: <channel x channel x frequency x time>
    %
    % Implementation of PLV as introduced by Lachaux et al. (1999)
    % Reference paper:
    %   JP Lachaux, E. Rodriguez, J. Martinerie, and FJ Varela.
    %   Measuring phase synchrony in brain signals.
    %   Human brain mapping, 8(4):194-208, 1999.
    %
    % Author: Simon J. Houtman, October 2013
    % Department of Artifical Intelligence, University of Groningen

    if (nargin < 1)
        error('No input wavelet specified.');
    end;

    % Number of trials, channels, frequencies and time samples
    N_trials = size(wavelet.trialinfo,1);
    N_chans = length(wavelet.label);
    N_freqs = length(wavelet.freq);
    N_samples = length(wavelet.time);

    % Initialize the PLV matrix
    % Dimord: <channel x channel x frequency x timesteps>
    plv = zeros(N_chans,N_chans,N_freqs,N_samples);

    % Loop over all channel combinations and compute PLV
    % for all dimensions at once using matrix multiplication
    for chan1 = 1 : N_chans
        for chan2 = 1 : N_chans
            wavelet_channel1 = wavelet.fourierspctrm(1:N_trials,chan1,1:N_freqs,1:
                N_samples);
            wavelet_channel2 = wavelet.fourierspctrm(1:N_trials,chan2,1:N_freqs,1:
                N_samples);
            % Phase is found by using atan2
            phi_channel1 = atan2(imag(wavelet_channel1),real(wavelet_channel1));
            phi_channel2 = atan2(imag(wavelet_channel2),real(wavelet_channel2));
            phi_diff = phi_channel2 - phi_channel1;
            plv(chan1,chan2,1:N_freqs,1:N_samples) = abs((1/N_trials) * sum(exp(j*(
                phi_diff))));
        end
    end

    % Return the phase-locking values in Fieldtrip format
    PLV.label = wavelet.label;
    PLV.dimord = 'chan_chan_freq_time';
```

```
53      PLV.plvspctrm = plv;
54      PLV.freq = wavelet.freq;
55      PLV.time = wavelet.time;
56      PLV.dof = N_trials;
57  end
```

Appendix B: computePLS.m

Function to compute surrogate phase-locking values and phase-locking statistics. The input signal is a wavelet of an EEG signal in Fieldtrip format. Also, the number of permutations to compute surrogate phase-locking values can be set as a parameter. If the number of permutations is undefined, the default number of permutations is 200, as used by Lachaux et al. (1999). The output is a 2D-matrix containing the p-values for the phase-locking statistics of all channel combinations.

```
function pls = computePLS(wavelet,N_perm)
    % Computes phase-locking statistics for all <channel x channel> combinations
    % for a wavelet of an EEG signal in Fieldtrip format
    %
    % Input parameters:
    % wavelet = Morlet wavelet of EEG signal in Fieldtrip format
    % Dimord of input wavelet: <trials x channel x frequency x time>
    % N_perm = Number of permutations to compute surrogate phase-locking values
    % default of N_perm is 200.
    %
    % Output parameters:
    % PLS = matrix with phase-locking statistics for every channel combination
    % Dimord of PLS: <channel x channel>
    %
    % Implementation of PLV and PLS as introduced by Lachaux et al. (1999)
    % Reference paper:
    %   JP Lachaux, E. Rodriguez, J. Martinerie, and FJ Varela.
    %   Measuring phase synchrony in brain signals.
    %   Human brain mapping, 8(4):194-208, 1999.
    %
    % Author: Simon J. Houtman, October 2013
    % Department of Artifical Intelligence, University of Groningen

    if (nargin < 1)
        error('No input wavelet specified.');
    end;

    if (nargin < 2)
        % Default number of permuatations to compute surrogate PLVs is 200
        N_perm = 200;
    end;

    % Compute original phase-locking values
    PLV = computePLV(wavelet);
    PLV = nanmean(PLV.plvspctrm,4);
    PLV = nanmean(PLV,3);

    % Number of trials, channels, frequencies and time samples
    N_trials = size(wavelet.trialinfo,1);
    N_chans = length(wavelet.label);
    N_freqs = length(wavelet.freq);
    N_samples = length(wavelet.time);

    % Loop over all channel combinations and compute surrogate PLV
    % for all dimensions at once using matrix multiplication
    % Initialize pls matrix
    pls = zeros(N_chans,N_chans);
    for chan1 = 1 : N_chans
        for chan2 = 1 : N_chans
            surrogate_plv = zeros(N_perm,1);
            % Compute N_perm surrogate phase locking values
            for perm = 1 : N_perm
```

```
53                  % Permutation array of the trials
54                  permuted_trials = randperm(N_trials);
55                  wavelet_channel1 = wavelet.fourierspctrm(1:N_trials,chan1,1:N_freqs,1:
                        N_samples);
56                  % Trials are permuted for the second channel
57                  wavelet_channel2 = wavelet.fourierspctrm(permuted_trials(1:N_trials),
                        chan2,1:N_freqs,1:N_samples);
58                  % Phase is found by using atan2
59                  phi_channel1 = atan2(imag(wavelet_channel1),real(wavelet_channel1));
60                  phi_channel2 = atan2(imag(wavelet_channel2),real(wavelet_channel2));
61                  % Compute the phase difference
62                  phi_diff = phi_channel2 - phi_channel1;
63                  % Compute the surrogate phase-locking values
64                  PLV_surr = abs((1/N_trials) * sum(exp(j*(phi_diff))));
65                  PLV_surr = nanmean(PLV_surr,4);
66                  PLV_surr = nanmean(PLV_surr,3);
67                  % Store the PLV_surr for every permutation
68                  surrogate_plv(perm) = PLV_surr;
69              end
70              % Compute the phase-locking statistic for every channel combination
71              % pls = % of surrogate values bigger than the original phase-locking value
72              pls(chan1,chan2) = sum(PLV(chan1,chan2)<=surrogate_plv)/N_perm;
73          end
74      end
75
76      % Return the phase-locking statistics
77      PLS.label = wavelet.label;
78      PLS.dimord = 'chan_chan';
79      PLS.pls = pls;
80      PLS.freq = mean(wavelet.freq);
81      PLS.time = wavelet.time;
82      PLS.dof = N_trials;
83  end
```